COBEM 2021 26th International Congress of Mechanical Engineering
ABCM Associação Brasileira de Engenharia e Ciências Mecânicas
November 22-26, 2021, Virtual Congress, Brazil

COB-2021-0722
SCREW BASED STATIC ANALYSIS OF A 4-DoF 3T1R FULLY DECOUPLED PARALLEL MANIPULATOR

Paulo Rossi
Rodrigo Cerqueira de Campos
Universidade Federal de Santa Catarina, Florianópolis SC 88040-900, Brazil
paulo.rossi@posgrad.ufsc.br
rodrigo.c.campos@posgrad.ufsc.br

Roberto Simoni
Andrea Piga Carboni
Universidade Federal de Santa Catarina, Joinville SC 89219-600, Brazil

Abstract. *The kinematic and static or kinetostatic analysis of parallel manipulators (PMs) is a critical parameter, especially for machining applications, due to the high-intensity forces. This paper aims to conduct a kinetostatic analysis of the 4-DoF 3T1R fully decoupled PM considering machining applications' operational forces. An analytical kinetostatic analysis is performed through a combination of natural coordinates (NC) and Davies' method. The NC method consists in defining points and vectors throughout the manipulator's links and joints. Afterward, by defining vector-loop equations starting from a known point, it is feasible to calculate every joint's position through the NC method. Additionally, employing a numerical method, it is achievable to compute the joints' positions. Therefore, applying the obtained results as inputs for the static analysis, it is possible to formulate the network action matrix through the screw theory applied to Davies' method. Ultimately, eliminating the linear dependent variables makes it possible to reach the magnitude vector concerning the operational forces and moments. Since the kinetostatic analytical model is determined, a comparison regarding a numerical finite element analysis (FEA) developed through a CAD model is performed. The analytical model presented a mean error of* 3.47% *regarding the output torque and indicated a one-to-one correspondence between the input and output forces. The 4-DoF 3T1R PMs, like the studied one, may represent a practical alternative for both widely used machining centers and machining robots. Decoupled architecture presents a straightforward kinematic analysis, trivial workspace volume, decoupled motions, and well-conditioned performance indices. These properties are desirable for machining applications. The analytical kinetostatic model is validated by comparing its results with the FEA, indicating how reliable is the 4-DoF 3T1R fully decoupled PM regarding the machining effort.*

Keywords: *parallel manipulator, stiffness analysis, screw theory, Davies method, Schönflies motion.*

1. INTRODUCTION

Parallel manipulators (PMs) are extensively used in various applications such as industry, medical, assembly tools, and machining centers. Compared to serial kinematic mechanisms, PMs have the advantages of high stiffness, fast response speed, high bearing capacity, high modularisation, and the centralized actuators layout (Tian *et al.*, 2019).

Traditionally, industrial machining robots have serial topology, which has a low carrying capacity. Thus, serial robots can not meet the large axial resistance requirements for some machining applications (Cui *et al.*, 2020). In turn, the PMs are progressively used in industrial machining applications such as trimming, drilling, and polishing on composite parts, including deburring, grinding, and milling on metal parts. Furthermore, these kinds of manipulators are generally able to perform various machining tasks, costing less than the traditional machining tools (Verl *et al.*, 2019).

Among the PMs for machining applications, the established five-axis machine tools provide numerous solutions for the machining problems and demands. However, these machines are costly and have some drawbacks, e.g., the limited end-effector spindle range and workspace capacity (Pandilov and Dukovski, 2012). Moreover, five-axis machine tools typically have complex kinematics. Consequently, the performance indices may vary considerably according to the operational workspace region and distinct directions at a given point. The 4-DoF 3T1R or Schönflies motion PMs may represent a practical compromise among the traditional PMs machining tools. The 4-DoF 3T1R PMs typically have straightforward kinematics, simple topologies, and well-conditioned performance indices, therefore overcoming some of the mentioned disadvantages of traditional machining tools.

It is essential to comprehend the external forces and torques' effects on the manipulators' end-effector displacements. The stiffness modeling and analysis has drawn academia's attention as a research area, impacting the machine design

in the preliminary and final stages (Lian *et al.*, 2015). The kinematic and static, also known as kinetostatic, analyses of PMs are fundamental steps to develop the stiffness modeling and further analysis. Through the kinetostatic model, the manipulator's performance indices can be achieved, aiding the machine's adjusting as desired (Huang *et al.*, 2020).

Lian *et al.* (2015) formulated the stiffness model of a 5-DoF PM for micromachining applications using the semi-analytical approach and considering the gravitational effects. The obtained model was validated with a stiffness experiment. Rossi *et al.* (2021a) presented a stiffness comparison between both a traditional 3-axis parallel CNC and a novel 4-DoF 3T1R PM for machining tasks. The author calculated these architectures' global stiffness index to indicate the machines' theoretical stiffness, an important parameter to evaluate the topology's potential for manufacturing applications. Zhao *et al.* (2020) established the stiffness model of 3RRlS and n(3RRlS) reconfigurable series-parallel manipulators, using a specific method that comprises the three main methods for stiffness analysis. Wei and Dai (2018) synthesized metamorphic joints to reach the desirable motion employing the Lie group method and differential geometry theory. Tian *et al.* (2019) proposed a new metamorphic PM for rescue applications which presents a novel rotatable-axis revolute joint, and his study was based mainly on the workspace and stiffness analysis. Moosavian and Xi (2014) introduced a new reconfigurable PMs family with lower instantaneous mobility, and the design of these machines focuses on the enhanced static and stiffness with minimal actuators number.

One of the critical characteristics that a machining robot may have is the capacity to undergo cutting forces, maintaining stable dynamics without significant deformation. These forces are due to the interaction of the workpiece and the manipulator's end-effector (Aydın *et al.*, 2014). Several researchers developed systematic manners to precisely evaluate the cutting forces present in some machining applications. Mebrahitom *et al.* (2017) demonstrated a numerical FEA predicting cutting forces of side milling operation, and the model considers both material and tool cutter properties. Additionally, cutting forces obtained from the computational simulations were compared to the experimental data. Phan *et al.* (2020) proposed a fuzzy control law system based on simple linear algebra computations; this control law calculates and determines the input forces of the actuated joints. The author carried out a comparative analysis between the fuzzy and another accurate controller. Kaymakci *et al.* (2012) presented a unified analytical model for cutting forces prediction in several machining applications as turning, milling, boring, and drilling operations. The author was based on geometric, kinematic, and mechanics to develop the model with a relatively low mean error.

Encouraged by the recent developments and importance concerning the kinetostatic analysis and intending to overcome the mentioned traditional machining PMs drawbacks, this paper aims to provide the analytical kinetostatic model and analysis of a decoupled motion 4-DoF 3T1R PM. Furthermore, this study considers that the PM will be employed in machining applications. Thus, the predicted cutting forces given by some authors serve as the model's inputs. Computational tests will be conducted, and then comparing the developed model results with FEA. This manuscript is organized as follows: Section 2. will detail the PM itself with its design and kinematic characteristics, and then the position kinematics is calculated. Section 3.1 and Section 3.2 formulates the static model and computes its analysis, respectively. Finally, in Section 4. some conclusions and future works are drawn.

2. DECOUPLED 4-DoF PM DESCRIPTION AND KINEMATIC ANALYSIS

This section will initially describe the studied 4-DoF 3T1R PM, henceforth known as "decoupled architecture," including structural and kinematic properties. Furthermore, the kinematic analysis will be conducted, in which the natural coordinates method was used to solve the problem through the inverse kinematic analysis.

2.1 Decoupled 4-DoF PM description

The decoupled architecture was initially proposed by Gogu (2013). The functional representation of such an architecture can be seen in Fig. 1, including its graph representation. The author synthesized this topology systematically and then classified it as belonging to the family named "Fully-Parallel Topologies with Decoupled Schönflies Motion". Thus, the decoupled architecture has the well-known 4-DoF 3T1R or Schönflies motion. Hence, it can translate along the three oriented Cartesian axes and rotate about one specific axis. All family architectures have four limbs (G_i, $i = 1, 2, 3, 4$) that connect the fixed base to the moving platform, which may or may not share the same topology. Since the number of actuators is equal to four, considering the Schönflies motion, there is no structural redundancy. Each limb has one actuated pair that can be a translational or revolute joint type, and the actuated pair is always located on the fixed link, reducing the system's inertia and maximizing the workspace volume.

As its name implies, the decoupled architecture has decoupled motions, i.e., the translational and rotational displacements depend on only one, or at least, two joints velocities. In that case, the translational motions depend on one actuated joint velocity $\mathbf{V}_i = \mathbf{V}_i(\dot{\mathbf{q}}_i)$, $i = 1, 2, 3$, and the rotational velocity on two actuated joints velocities $\phi = \phi(\dot{\mathbf{q}}_3, \dot{\mathbf{q}}_4)$. This fact leads to a triangular Jacobian matrix. The connectivity of the decoupled architecture's limbs G_2, G_3, and G_4 is equal to four, and one for G_1 limb, as well as their mobility. These limbs also include one planar parallelogram (P_a) joint, that is, a joint which combines four revolute joints and four links, similar to a four-bar mechanism. G_1 limb has four degrees of mobility, and it rotates about the X axis. G_2, G_3, and G_4 possess five degrees of mobility, and they can rotate about

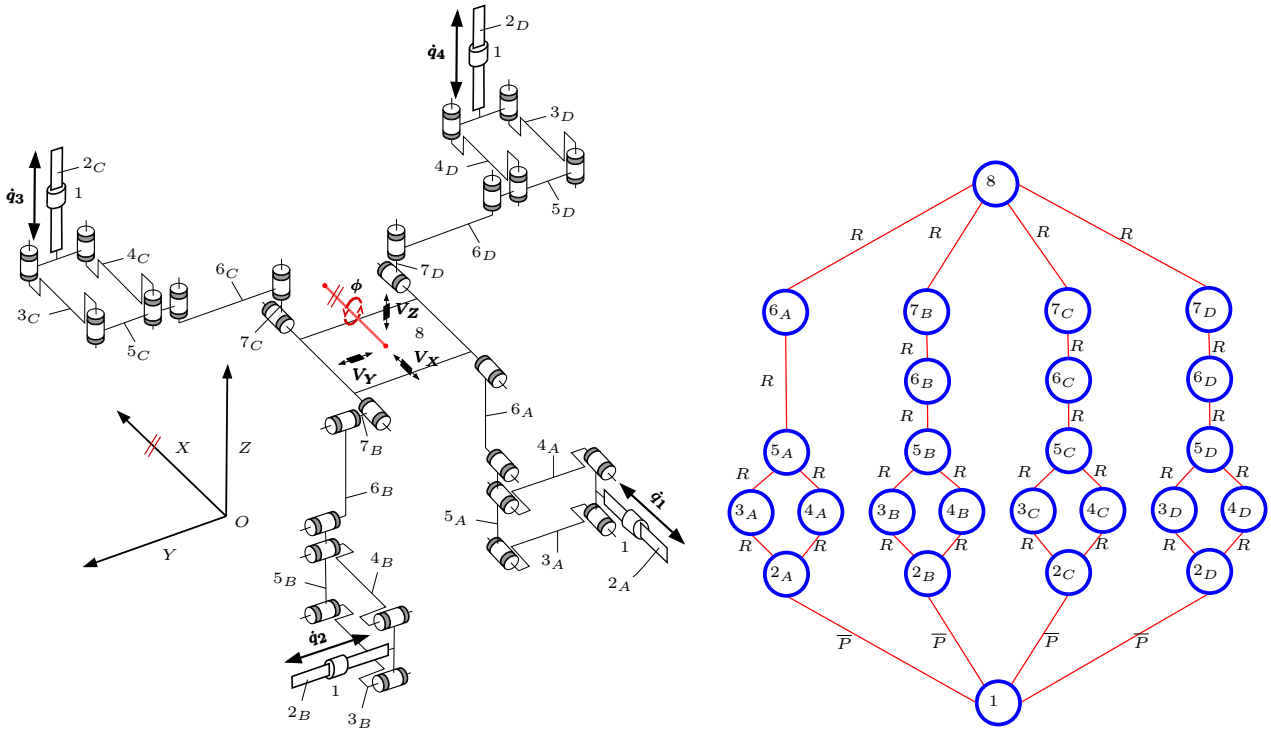

Figure 1: (a) Decoupled architecture topology, and (b) its graph representation.

both X and Y axes. Some connecting conditions must be respected to assemble the manipulator. Namely, the last revolute joints should have their axes parallel, and the actuated prismatic joint of limbs G_1, G_2, and G_3 must have perpendicular directions; furthermore, the G_3 and G_4 limbs actuated translational pair should have parallel directions.

Regarding the decoupled architecture itself, it consists of 25 links and 31 joints, combined in three identical limbs and one slightly different. The rotational motion of this topology is about the X Cartesian axis, and all the actuators are prismatic pairs type. There are three closed kinematic loops, and the connectivity is equal to four between the fixed and moving platforms. The decoupled architecture has the topology $3\overline{P}P_aRRR{-}1\overline{P}P_aRR$, where the overlines and numerals mean the actuated joints and the total limbs' number, respectively. Three limbs initiate with a prismatic actuator, followed by a planar parallelogram and three consecutive revolute joints. As mentioned, one limb is slightly different, with one less revolute joint, then only two consecutive revolute joints follow the planar parallelogram joint towards the end effector. Considering the decoupled architecture's limbs, their topologies arrangement can be represented as $\overline{P} \parallel P_a \parallel R \parallel R$ and $\overline{P} \parallel P_a \parallel R \parallel R \perp R$, where $\parallel$ and $\perp$ symbols indicate that the joints are parallel or orthogonal to each other, respectively. It can be concluded that the joints of each limb have all their axes parallel to each other, except for the G_1 limb, in which the last revolute joint is perpendicular to the previous one.

2.2 Kinematic analysis

The kinematic analysis of multibody systems is generally achieved through inverse kinematics using a geometrical approach, where a vector-loop equation is defined for each limb. This method has been successfully applied by several authors, such as Lian *et al.* (2015) who analyzed the stiffness of a 5-DoF PM. It presents, however, two major drawbacks. First, along with the procedure, all passive joint variables are eliminated. Although, these passive joint variables are necessary to perform the static analysis. Second, the high degree of nonlinearity of the governing equations results in a complex computer implementation (Xu *et al.*, 2021). In some cases, the direct kinematics can be applied depending on the analyzed architecture, especially those presenting simple topologies. Rossi *et al.* (2021b) developed the direct kinematics of the studied architecture in this paper, including its velocities, workspace, and singularities analyses. Nevertheless, this method has the same mentioned drawbacks.

As a mean to reduce the mathematical complexity of the resulting system of equations and get the coordinates of all passive joints, the direct kinematics was developed through Natural Coordinates (NC). From Fig. 2, the coordinates for points P and P_{iA} are known, as are the dimensions a_1, a_2, l_1, and l_2. Hence, the coordinates for P_1, P_2, P_3, and P_4 can

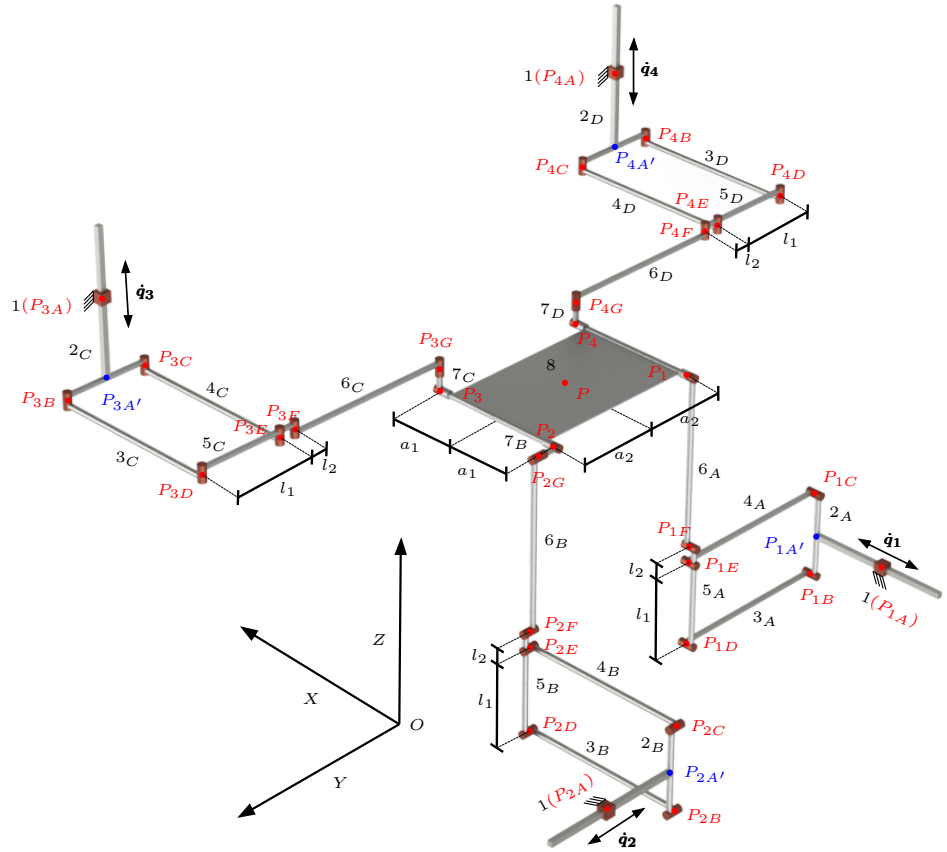

Figure 2: Decoupled manipulator functional representation.

be calculated by

$$\mathbf{P_1} = \mathbf{P} + \begin{bmatrix} -a_1 \\ -a_2 \\ 0 \end{bmatrix}, \mathbf{P_2} = \mathbf{P} + \begin{bmatrix} -a_1 \\ a_2 \\ 0 \end{bmatrix}, \mathbf{P_3} = \mathbf{P} + \begin{bmatrix} a_1 \\ a_2 \\ 0 \end{bmatrix}, \mathbf{P_4} = \mathbf{P} + \begin{bmatrix} a_1 \\ -a_2 \\ 0 \end{bmatrix}. \tag{1}$$

Additionally, decoupled architecture can perform a rotational motion about the X axis. Thus, applying a simple rotation matrix around the X axis concerning the ϕ angle, it is possible to achieve the moving platform's position and orientation as stated below:

$$\mathbf{PP_i} = R_x(\phi)\mathbf{P_i} \Rightarrow \mathbf{PP_i} = \begin{bmatrix} 1 & 0 & 0 \\ 0 & cos(\phi) & -sin(\phi) \\ 0 & sin(\phi) & cos(\phi) \end{bmatrix} \mathbf{P_i}. \tag{2}$$

For limbs 2, 3, and 4, the coordinates for joints P_iG are also directly determined by

$$\mathbf{P_{2G}} = \mathbf{P_2} + \begin{bmatrix} 0 \\ L_7 \\ 0 \end{bmatrix}, \mathbf{P_{3G}} = \mathbf{P_3} + \begin{bmatrix} 0 \\ 0 \\ L_7 \end{bmatrix}, \mathbf{P_{4G}} = \mathbf{P_4} + \begin{bmatrix} 0 \\ 0 \\ L_7 \end{bmatrix}. \tag{3}$$

It can be seen that, for every limb, the coordinates for points $P_{iA'}$ can be calculated based on the input q_i, as in

$$\mathbf{P_{1A'}} = \mathbf{P_{1A}} + \begin{bmatrix} q_1 \\ 0 \\ 0 \end{bmatrix}, \mathbf{P_{2A'}} = \mathbf{P_{2A}} + \begin{bmatrix} 0 \\ q_2 \\ 0 \end{bmatrix}, \mathbf{P_{3A'}} = \mathbf{P_{3A}} + \begin{bmatrix} 0 \\ 0 \\ q_3 \end{bmatrix}, \mathbf{P_{4A'}} = \mathbf{P_{4A}} + \begin{bmatrix} 0 \\ 0 \\ q_4 \end{bmatrix}, \tag{4}$$

and since $P_{iA'}$ is always collinear to joints P_{iB} and P_{iC}, regardless of the moving platform's position and orientation, it can be stated that

$$\mathbf{P_{1B}} = \mathbf{P_{1A'}} + \begin{bmatrix} 0 \\ 0 \\ -\frac{l_1}{2} \end{bmatrix}, \mathbf{P_{2B}} = \mathbf{P_{2A'}} + \begin{bmatrix} 0 \\ 0 \\ -\frac{l_1}{2} \end{bmatrix}, \mathbf{P_{3B}} = \mathbf{P_{3A'}} + \begin{bmatrix} 0 \\ \frac{l_1}{2} \\ 0 \end{bmatrix}, \mathbf{P_{4B}} = \mathbf{P_{4A'}} + \begin{bmatrix} 0 \\ -\frac{l_1}{2} \\ 0 \end{bmatrix}. \tag{5}$$

$$\mathbf{P_{1C}} = \mathbf{P_{1A'}} + \begin{bmatrix} 0 \\ 0 \\ \frac{l_1}{2} \end{bmatrix}, \mathbf{P_{2C}} = \mathbf{P_{2A'}} + \begin{bmatrix} 0 \\ 0 \\ \frac{l_1}{2} \end{bmatrix}, \mathbf{P_{3C}} = \mathbf{P_{3A'}} + \begin{bmatrix} 0 \\ -\frac{l_1}{2} \\ 0 \end{bmatrix}, \mathbf{P_{4C}} = \mathbf{P_{4A'}} + \begin{bmatrix} 0 \\ \frac{l_1}{2} \\ 0 \end{bmatrix}. \tag{6}$$

The same principle can be adopted to determine the coordinates of joints P_{iD}, P_{iE}, and P_{iF}, which are also always collinear. Hence,

$$\mathbf{P_{1E}} = \mathbf{P_{1F}} + \begin{bmatrix} 0 \\ 0 \\ -l_2 \end{bmatrix}, \mathbf{P_{2E}} = \mathbf{P_{2F}} + \begin{bmatrix} 0 \\ 0 \\ -l_2 \end{bmatrix}, \mathbf{P_{3E}} = \mathbf{P_{3F}} + \begin{bmatrix} 0 \\ l_2 \\ 0 \end{bmatrix}, \mathbf{P_{4E}} = \mathbf{P_{4F}} + \begin{bmatrix} 0 \\ -l_2 \\ 0 \end{bmatrix}. \tag{7}$$

$$\mathbf{P_{1D}} = \mathbf{P_{1E}} + \begin{bmatrix} 0 \\ 0 \\ -l_1 \end{bmatrix}, \mathbf{P_{2D}} = \mathbf{P_{2E}} + \begin{bmatrix} 0 \\ 0 \\ -l_1 \end{bmatrix}, \mathbf{P_{3D}} = \mathbf{P_{3E}} + \begin{bmatrix} 0 \\ l_1 \\ 0 \end{bmatrix}, \mathbf{P_{4D}} = \mathbf{P_{4E}} + \begin{bmatrix} 0 \\ -l_1 \\ 0 \end{bmatrix}. \tag{8}$$

As a result, for each limb there are three independent unknowns, two elements of $\mathbf{P_{iF}}$ and q_i. Thus, it is necessary a system composed of three equations per limb. Applying the Natural Coordinates procedure, the following system of equations are obtained,

$$\begin{cases} (x_{P_{1B}} - x_{P_{1D}})^2 + (y_{P_{1B}} - y_{P_{1D}})^2 + (z_{P_{1B}} - z_{P_{1D}})^2 = L_{3A}^2 \\ (x_{P_{1C}} - x_{P_{1E}})^2 + (y_{P_{1C}} - y_{P_{1E}})^2 + (z_{P_{1C}} - z_{P_{1E}})^2 = L_{4A}^2 \\ (x_{P_{1F}} - x_{P_1})^2 + (y_{P_{1F}} - y_{P_1})^2 + (z_{P_{1F}} - z_{P_1})^2 = L_{6A}^2. \end{cases} \tag{9}$$

$$\begin{cases} (x_{P_{iB}} - x_{P_{iD}})^2 + (y_{P_{iB}} - y_{P_{iD}})^2 + (z_{P_{iB}} - z_{P_{iD}})^2 = L_{3A}^2 \\ (x_{P_{iC}} - x_{P_{iE}})^2 + (y_{P_{iC}} - y_{P_{iE}})^2 + (z_{P_{iC}} - z_{P_{iE}})^2 = L_{4A}^2 \\ (x_{P_{iF}} - x_{P_{iG}})^2 + (y_{P_{iF}} - y_{P_{iG}})^2 + (z_{P_{iF}} - z_{P_{iG}})^2 = L_{6A}^2. \end{cases} \tag{10}$$

Since Eq. (9) and Eq. (10) are nonlinear, it is not possible to solve them analytically. Therefore, the Newton-Raphson numerical method is adopted to solve this system of equations for each limb. The method described in this section was developed in Python, and the results were validated through a CAD model of the PM.

3. STATIC ANALYSIS

This section first describes the 4-DoF 3T1R PM static modeling using a screw theory rationale as Davies' method describes. Finally, the developed model's results were calculated and compared with the FEA method to validate them, as discussed in the next section.

3.1 Static model

The static analysis consists of determining the reaction forces and torques on each joint of a mechanism. It is generally based on the solution of a system of equilibrium equations defined by the topology. The static equilibrium depends on the existence of external inputs generated by actuators, as well as external actions applied on the end-effector (Davies, 2000). For the static analysis of the PM through Davies method, the external forces acting on the moving platform, as well as the forces generated by the actuators must be internalized, which results in a super-constrained configuration.

Let λ be the number of DoFs of the workspace, and since the studied PM is a spatial mechanism, then $\lambda = 6$. The wrench \$ of a joint is a $\lambda \times C_{joint}$ matrix, where C_{joint} represents the number of constraints imposed by the joint, in which each column contains the λ unit action coordinates of the restraint action, as explained by Davies (2000). It can be seen from Fig. 2 that the PM is composed only of revolute joints and prismatic actuators. Hence, $C_{joint} = 5$ for every passive joint, which wrenches results in 6×5 matrices, and are presented by Eq. (11). The subscripts x, y, and z represent the freedom of rotation around the X, Y, and Z axes. It should be noted that the actuation is considered an additional constraint for the actuated prismatic joints. Therefore, the wrenches that represent the actuated joints are 6×6 matrices, represented by Eq. (12).

$$\$_{\mathbf{x}} = \begin{bmatrix} 0 & -z_{joint} & y_{joint} & 0 & 0 \\ z_{joint} & 0 & -x_{joint} & 1 & 0 \\ -y_{joint} & x_{joint} & 0 & 0 & 1 \\ 1 & 0 & 0 & 0 & 0 \\ 0 & 1 & 0 & 0 & 0 \\ 0 & 0 & 1 & 0 & 0 \end{bmatrix}, \$_{\mathbf{y}} = \begin{bmatrix} 0 & -z_{joint} & y_{joint} & 1 & 0 \\ z_{joint} & 0 & -x_{joint} & 0 & 0 \\ -y_{joint} & x_{joint} & 0 & 0 & 1 \\ 1 & 0 & 0 & 0 & 0 \\ 0 & 1 & 0 & 0 & 0 \\ 0 & 0 & 1 & 0 & 0 \end{bmatrix},$$

$$\$_{\mathbf{z}} = \begin{bmatrix} 0 & -z_{joint} & y_{joint} & 1 & 0 \\ z_{joint} & 0 & -x_{joint} & 0 & 1 \\ -y_{joint} & x_{joint} & 0 & 0 & 0 \\ 1 & 0 & 0 & 0 & 0 \\ 0 & 1 & 0 & 0 & 0 \\ 0 & 0 & 1 & 0 & 0 \end{bmatrix}. \tag{11}$$

$$\$_{\mathbf{a}} = \begin{bmatrix} 0 & -z_{PiA} & y_{PiA} & 1 & 0 & 0 \\ z_{PiA} & 0 & -x_{PiA} & 0 & 1 & 0 \\ -y_{PiA} & x_{PiA} & 0 & 0 & 0 & 1 \\ 1 & 0 & 0 & 0 & 0 & 0 \\ 0 & 1 & 0 & 0 & 0 & 0 \\ 0 & 0 & 1 & 0 & 0 & 0 \end{bmatrix}. \tag{12}$$

As stated above, the external forces acting on the moving platform must be internalized. Considering the application of a force along each axis of the coordinate system (F_x, F_y, and F_z), the wrench for external load applied on point P is given by

$$\$_{\mathbf{F_{EL}}} = \begin{bmatrix} 0 & -z_p & y_p & 1 \\ z_p & 0 & -x_p & 0 \\ -y_p & x_p & 0 & 0 \\ 1 & 0 & 0 & 0 \\ 0 & 1 & 0 & 0 \\ 0 & 0 & 1 & 0 \end{bmatrix}. \tag{13}$$

The equilibrium equations are achieved from a directed graph representation of the mechanism topology, presented by Fig. 3, where the dashed red lines represent the chords, the black lines represent the branches, the blue lines are the forces generated by the actuators, and the green line is an external load applied to the moving platform.

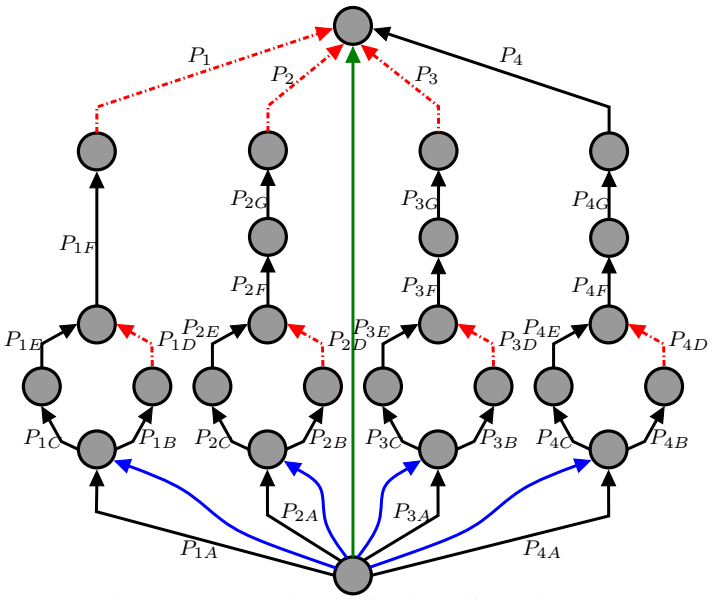

Figure 3: Decoupled manipulator directed graph.

The number of cuts k is equal to the number of edges, minus the number of independent loops. From Fig. 1b, it can be seen that the PM has 31 edges, and 7 loops, resulting in $k = 24$ cuts. Each cut may pass through any number of chords,

but must pass through a single branch. Let C be the total number of constraints imposed by the joints. From Fig. 2, we have four actuated prismatic joints, with 6 constraints each, and 27 passive revolute joints, with 5 constraints each, which results in $C = 159$. The cutset matrix $\mathbf{Q}$ is composed of k rows and C columns, where each element $q_{i,j}$ may take on the values of 0, -1 or +1, following the pattern presented by

$$q_{i,j} = \begin{cases} 0, \text{if cut } i \text{ does not include edge } j; \\ +1, \text{if cut } i \text{ and edge } j \text{ shares the same direction;} \\ -1, \text{if cut } i \text{ and edge } j \text{ have opposite directions.} \end{cases} \tag{14}$$

Due to the size of this matrix, it is shown only partially by

$$\mathbf{Q} = \begin{array}{c} \\ P_{1A} \\ P_{1B} \\ P_{1C} \\ P_{1E} \\ P_{1F} \\ \vdots \\ P_4 \end{array} \begin{array}{c} \begin{array}{cccccccc} F_{xP_1} & F_{yP_1} & F_{zP_1} & T_{yP_1} & \dots & F_{yEL} & F_{zEL} & T_{xEL} \end{array} \\ \begin{bmatrix} -1 & -1 & -1 & -1 & \dots & 0 & 0 & 0 \\ 0 & 0 & 0 & 0 & \dots & 0 & 0 & 0 \\ -1 & -1 & -1 & -1 & \dots & 0 & 0 & 0 \\ -1 & -1 & -1 & -1 & \dots & 0 & 0 & 0 \\ 0 & 0 & 0 & 0 & \dots & 0 & 0 & 0 \\ \vdots & \vdots & \vdots & \vdots & \ddots & \vdots & \vdots & \vdots \\ 0 & 0 & 0 & 0 & \dots & 0 & 0 & 0 \end{bmatrix} \end{array}. \tag{15}$$

Further details about the construction method of the cutset matrix can be found in Davies (2000).

The wrenches defined in Eq. (11), Eq. (12), and Eq. (13) can be bound together in a single unit action matrix $\mathbf{A_D}$. This matrix is constructed by arranging first the chord wrenches, followed by the branch wrenches, as in

$$\begin{aligned} \mathbf{A_D} = [&\$_{\mathbf{P_1}} \quad \$_{\mathbf{P_{1D}}} \quad \$_{\mathbf{P_2}} \quad \$_{\mathbf{P_{2D}}} \quad \$_{\mathbf{P_3}} \quad \$_{\mathbf{P_{3D}}} \quad \$_{\mathbf{P_{4D}}} \quad \$_{\mathbf{P_{1A}}} \quad \$_{\mathbf{P_{1B}}} \quad \dots \\ &\dots \quad \$_{\mathbf{P_{1C}}} \quad \$_{\mathbf{P_{1E}}} \quad \$_{\mathbf{P_{1F}}} \quad \$_{\mathbf{P_{2A}}} \quad \$_{\mathbf{P_{2B}}} \quad \$_{\mathbf{P_{2C}}} \quad \$_{\mathbf{P_{2E}}} \quad \$_{\mathbf{P_{2F}}} \quad \dots \\ &\dots \quad \$_{\mathbf{P_{2G}}} \quad \$_{\mathbf{P_{3A}}} \quad \$_{\mathbf{P_{3B}}} \quad \$_{\mathbf{P_{3C}}} \quad \$_{\mathbf{P_{3E}}} \quad \$_{\mathbf{P_{3F}}} \quad \$_{\mathbf{P_{3G}}} \quad \$_{\mathbf{P_{4A}}} \quad \dots \\ &\dots \quad \$_{\mathbf{P_{4B}}} \quad \$_{\mathbf{P_{4C}}} \quad \$_{\mathbf{P_{4E}}} \quad \$_{\mathbf{P_{4F}}} \quad \$_{\mathbf{P_{4G}}} \quad \$_{\mathbf{P_4}} \quad \$_{\mathbf{F_{EL}}}]. \end{aligned} \tag{16}$$

For a mechanism composed of k cuts and a λ workspace, it is possible to obtain λk equations, which must be satisfied in order to fully determine the statics. The full equilibrium system is obtained by binding each cutset matrix in a single Network Action Matrix $\mathbf{A_N}$, composed of λk rows and C columns. The $\mathbf{A_N}$ matrix is assembled by distributing the wrenches belonging to each cut, multiplying the unit action matrix $\mathbf{A_D}$ to each line of the cutset matrix $\mathbf{Q}$, as described by Cazangi *et al.* (2008). The assembling method is presented

$$\mathbf{Q_1} = \begin{bmatrix} q_{1,1} & q_{1,2} & q_{1,3} & \dots & q_{1,C} \end{bmatrix}, \tag{17}$$

$$diag\{\mathbf{Q_1}\} = \begin{bmatrix} q_{1,1} & 0 & 0 & \dots & 0 \\ 0 & q_{1,2} & 0 & \dots & 0 \\ 0 & 0 & q_{1,3} & \dots & 0 \\ \vdots & \vdots & \vdots & \ddots & \vdots \\ 0 & 0 & 0 & \dots & q_{1,C} \end{bmatrix}, \tag{18}$$

$$\mathbf{A_N} = \begin{bmatrix} \mathbf{A_{D}}_{\lambda,C} diag\{\mathbf{Q_1}\} \\ \mathbf{A_{D}}_{\lambda,C} diag\{\mathbf{Q_2}\} \\ \vdots \\ \mathbf{A_{D}}_{\lambda,C} diag\{\mathbf{Q_k}\} \end{bmatrix}. \tag{19}$$

To satisfy the cutset law, the sum of all wrenches belonging to the same cut must be equal to zero. Therefore, the matrix $\mathbf{A_{N}}_{\lambda k,C}$ multiplied by the action magnitude vector $\mathbf{\Psi}_{C,1}$ is equal to zero, as presented by

$$\mathbf{A_{N}}_{\lambda k,C} \mathbf{\Psi}_{C,1} = \overrightarrow{\mathbf{0}}_{C,1}. \tag{20}$$

Equation (20) is only solvable if matrix $\mathbf{A_N}$ is square. However, for an overconstrained mechanism (in which every external force is internalized), there is a required number of known variables C_n to fully define the mechanism, calculated by

$$C_n = C - \lambda k, \tag{21}$$

which, for the studied PM, results in $C_n = 15$.

In order to solve the statics, Eq. (20) must be manipulated, dividing the network action matrix in a primary $\mathbf{A_{N_p}}$ matrix, composed of the known variables wrenches, and secondary $\mathbf{A_{N_s}}$ network action matrix, composed of the unknown variables wrenches. The magnitude vector Ψ is also divided in primary Ψ_p and secondary Ψ_s magnitude vectors. This way, Eq. (20) is transformed to

$$\mathbf{A_{N_s}}_{\lambda k,\lambda k}\mathbf{\Psi_s}_{\lambda k,1} = -\mathbf{A_{N_p}}_{\lambda k,C_n}\mathbf{\Psi_p}_{C_n,1}. \tag{22}$$

3.2 Static analysis and validation

The method presented above was developed in Python. Even though the number of known variables does not match the requirements imposed by Eq. (21), the problem is solvable by the least-squares solution approach. This method computes the vector $\mathbf{x}$ that approximately solves the system of equations in the form of $\mathbf{Ax} = \mathbf{b}$, and can be implemented through the *numpy.linalg.lstsq* python package.

The validation of the results obtained from the method presented in this paper is achieved by a Finite Element Analysis, which was performed for a set of different positions of the moving platform. Here, the support for joints P_{iA} are fixed, and the prismatic joint is free to translate along the respective axis with a frictionless contact. The forces that represent the input of the actuators are applied at the end of the prismatic rod. All revolute joints were modelled as frictionless pin joints. Finally, the motion of the moving platform was completely restricted. The output forces and torques of the moving platform for a set of inputs are measured by computing the reactions of the moving platform constraints. Fig. 4 illustrates the designed FEA model for the second case ($X = 0$, $Y = 0$, $Z = 0$, $\phi = 30°$) described in Tab. 1. This case and the other ones follow the same rationale as described above.

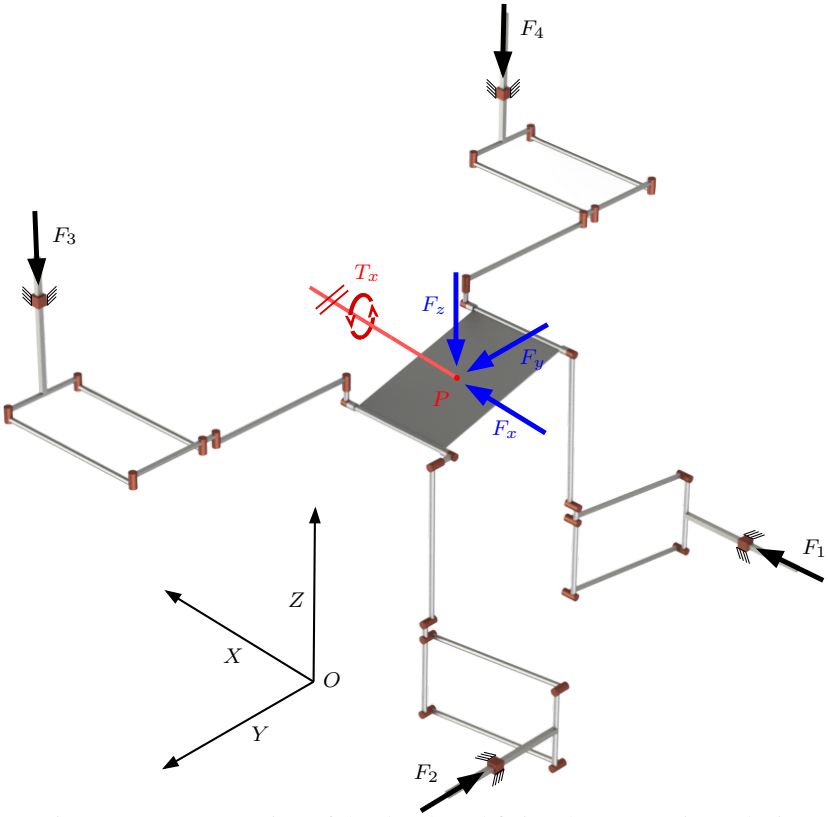

Figure 4: Representation of the developed finite element static analysis.

Both developed analytical and FEA static models were implemented using real measured forces concerning milling machining operations. Kaymakci *et al.* (2012) proposed a unified analytical model to predict cutting forces in a sort of machining operations. Examining the decoupled architecture topology as exposed in Fig. 2, one can note that it has the potential to perform some machining tasks such as milling and drilling. For this reason, it will be used forces related to the milling operations, which are taken from Kaymakci *et al.* (2012).

There are a series of tasks that can be executed in a milling machine. This paper will consider operational forces generated by both slotting and quarter immersion down milling. The used forces to implement the analytical model were experimentally tested by Kaymakci *et al.* (2012), varying the machining parameters. The slotting tests were carried out with $N = 700$ rpm, $a = 5$ mm (depth of cut), and $f = 0.1$ to 0.2 mm/tooth (feed rate). While the quarter immersion down milling utilized $N = 350$ to 1000 rpm, $a = 20$ to 30 mm, and $f = 0.2$ mm/tooth. Adopting the exposed parameters, the

authors obtained maximum forces of $F_x = -600$ to 750 N, $F_y = -250$ to 1500 N, and $F_z = -250$ N. The computational tests of the developed static models are made considering some moving platform's positions and orientations, and the obtained results are exposed in Tab. 1.

Table 1: Statics analytical model results compared to the FEA model.

Coordinates [mm]	**Input forces** [N]	**Davies' method**	**FEA analysis**
$X = 0, Y = 0$	$F_1 = 750, F_2 = 1500$	$F_x = -750\ N, F_y = -1500\ N$	$F_x = -750\ N, F_y = -1500\ N$
$Z = 0, \phi = 0°$	$F_3 = 150, F_4 = 150$	$F_z = -300\ N\ T_x = 0\ Nm$	$F_z = -300\ N, T_x = 0\ Nm$
$X = 0, Y = 0$	$F_1 = 750, F_2 = 1500$	$F_x = -750\ N, F_y = -1500\ N$	$F_x = -750\ N, F_y = -1500\ N$
$Z = 0, \phi = 30°$	$F_3 = 150, F_4 = 150$	$F_z = -300\ N\ T_x = 225\ Nm$	$F_z = -300\ N, T_x = 217\ Nm$
$X = -200, Y = -50$	$F_1 = 750, F_2 = 1500$	$F_x = -750\ N, F_y = -1500\ N$	$F_x = -750\ N, F_y = -1500\ N$
$Z = 0, \phi = 15°$	$F_3 = 150, F_4 = 150$	$F_z = -300\ N\ T_x = -102\ Nm$	$F_z = -300\ N, T_x = -109\ Nm$

One attractive fact regarding the decoupled architecture is that each manipulator's limbs only offer forces constraints (F_x, F_y, F_z) along the actuated translational pair axis. In other words, each limb restricts forces only in one direction, namely, the direction of its actuated joint axis. The first limb, for example, has its actuated pair axis parallel to the X Cartesian axis. Hence, this leads to the force constraints only regarding the X axis. Whether forces were applied on the moving platform in any other directions, these will not be restricted by the first limb as a whole. This characteristic exists because of the decoupled motion property and contributes to the direct forces distribution towards the actuators.

Due to the decoupled motion property, one can apply the same force in the corresponding actuator to compensate for the operational forces on the moving platform. Thus, the resulting forces in the moving platform regarding the applied forces in the translational actuators will be the same, whatever the analyzed position and orientation. Ultimately, the moving platform also has a rotational DoF around the X axis. Consequently, only the moving platform torque around the X axis varies according to the analyzed pose, considering the input forces. It can be concluded that the resulting torque in the X axis has a mean percentage error of 3.47% concerning all studied cases, with a maximum error of 6.86%. All errors were calculated with respect to the analytical analysis developed through Davies' method.

4. CONCLUSIONS

Decoupled architecture has decoupled motions, presenting simple kinematics and statics. The kinematic model was developed employing the NC method, which leads to every manipulator's joint position. Since the joint's positions were known, it is possible to develop the Davies' method achieving the magnitude forces and torque vector as the analytical static model presents. Furthermore, a static FEA was designed to validate the analytical model. The analytical model has shown a mean error of 3.47%, only considering the output torque along with the X axis. No errors are presented concerning the output forces. As a result of the static model, one can note a one-to-one correspondence between the forces distribution due to the decoupled property of the architecture. Thus, decoupled architecture proves itself a good choice for machining applications, namely, for milling and drilling tasks considering its kinetostatic characteristics.

Additionally, the 4-DoF 3T1R PMs may represent a convenient choice among the traditional machining robots with either high complex kinematics or insufficient capacity to operate in some cases. In addition, decoupled architecture can execute relatively complex tasks with its spindle orientation capability with good performance indices, presenting a parallelepiped shape workspace. For future works, the geometrical synthesis of such architecture can be achieved based on the analytical kinetostatic model developed in this paper.

5. ACKNOWLEDGEMENTS

The authors would like to thank CAPES. Moreover, Rodrigo Cerqueira de Campos and Paulo Rossi are thankful to CAPES Foundation for financial support: Process number 88882.344684/2019-01 and 88887.357849/2019-00.

6. REFERENCES

Aydın, M., Uçar, M., Cengiz, A., Kurt, M. and Bakır, B., 2014. "A methodology for cutting force prediction in side milling". *Materials and Manufacturing Processes*, Vol. 29, No. 11-12, pp. 1429–1435.

Cazangi, H.R. *et al.*, 2008. "Aplicação do método de davies para análise cinemática e estática de mecanismos com múltiplos graus de liberdade".

Cui, G., Liu, J., Hu, Z., Zhang, Y. and Hou, H., 2020. "Performance analysis and optimization of a rigid-flexible parallel manipulator". *Proceedings of the Institution of Mechanical Engineers, Part C: Journal of Mechanical Engineering Science*, Vol. 234, No. 23, pp. 4620–4635.

Davies, T., 2000. "The 1887 committee meets again. subject: freedom and constraint".

Gogu, G., 2013. *Structural Synthesis of Parallel Robots: Part 5: Basic Overconstrained Topologies with Schönflies Motions*, Vol. 206. Springer Science & Business Media.

Huang, G., Zhang, D., Tang, H., Kong, L. and Song, S., 2020. "Analysis and control for a new reconfigurable parallel mechanism". *International Journal of Advanced Robotic Systems*, Vol. 17, No. 5, p. 1729881420931322.

Kaymakci, M., Kilic, Z. and Altintas, Y., 2012. "Unified cutting force model for turning, boring, drilling and milling operations". *International Journal of Machine Tools and Manufacture*, Vol. 54, pp. 34–45.

Lian, B., Sun, T., Song, Y., Jin, Y. and Price, M., 2015. "Stiffness analysis and experiment of a novel 5-DoF parallel kinematic machine considering gravitational effects". *International Journal of Machine Tools and Manufacture*, Vol. 95, pp. 82–96.

Mebrahitom, A., Choon, W. and Azhari, A., 2017. "Side milling machining simulation using finite element analysis: prediction of cutting forces". *Materials Today: Proceedings*, Vol. 4, No. 4, pp. 5215–5221.

Moosavian, A. and Xi, F.J., 2014. "Design and analysis of reconfigurable parallel robots with enhanced stiffness". *Mechanism and Machine Theory*, Vol. 77, pp. 92–110.

Pandilov, Z. and Dukovski, V., 2012. "Parallel kinematics machine tools: Overview-from history to the future". *Annals of the Faculty of Engineering Hunedoara*, Vol. 10, No. 2, p. 111.

Phan, K.B., Ha, H.T. and Hoang, S.V., 2020. "Eliminating the effect of uncertainties of cutting forces by fuzzy controller for robots in milling process". *Applied Sciences*, Vol. 10, No. 5, p. 1685.

Rossi, P., Simoni, R. and Carboni, A.P., 2021a. "Analysis of a 4-DOF 3T1R parallel robot for machining applications: A stiffness study". In *Advances in Industrial Machines and Mechanisms*, Springer, pp. 161–171.

Rossi, P., Simoni, R., Simas, H. and Carboni, A.P., 2021b. "Kinematic analysis of a 3T1R fully decoupled parallel manipulators family". In *International Symposium on Multibody Systems and Mechatronics*. Springer, pp. 102–109.

Tian, H.b., Ma, H.w., Xia, J., Ma, K. and Li, Z.z., 2019. "Stiffness analysis of a metamorphic parallel mechanism with three configurations". *Mechanism and Machine Theory*, Vol. 142, p. 103595.

Verl, A., Valente, A., Melkote, S., Brecher, C., Ozturk, E. and Tunc, L.T., 2019. "Robots in machining". *CIRP Annals*, Vol. 68, No. 2, pp. 799–822.

Wei, J. and Dai, J.S., 2018. "Group method for synthesis of metamorphic parallel mechanism with 1R2T and 2R1T reconfiguration". In *2018 International Conference on Reconfigurable Mechanisms and Robots (ReMAR)*. IEEE, pp. 1–6.

Xu, X., Luo, J., Feng, X., Peng, H. and Wu, Z., 2021. "A generalized inertia representation for rigid multibody systems in terms of natural coordinates". *Mechanism and Machine Theory*, Vol. 157, p. 104174.

Zhao, C., Guo, H., Zhang, D., Liu, R., Li, B. and Deng, Z., 2020. "Stiffness modeling of n (3RRlS) reconfigurable series-parallel manipulators by combining virtual joint method and matrix structural analysis". *Mechanism and Machine Theory*, Vol. 152, p. 103960.

7. RESPONSIBILITY NOTICE

The authors are solely responsible for the printed material included in this paper.